

# Analysis of Solids with Numerous Microcracks Using the Fast Multipole DBEM

P. B. Wang<sup>1</sup>, Z. H. Yao<sup>1,2</sup> and T. Lei<sup>1</sup>

**Abstract:** The fast multipole method (FMM) is applied to the dual boundary element method (DBEM) for the analysis of finite solids with large numbers of microcracks. The application of FMM significantly enhances the run-time and memory storage efficiency. Combining multipole expansions with local expansions, computational complexity and memory requirement are both reduced to  $O(N)$ , where  $N$  is the number of DOFs (degrees of freedom). This numerical scheme is used to compute the effective in-plane bulk modulus of 2D solids with thousands of randomly distributed microcracks. The results prove that the IDD method, the differential method, and the method proposed by Feng and Yu can give proper estimates. The effect of microcrack non-uniform distribution is evaluated, and the numerical results show that non-uniform distribution of microcracks increases the effective in-plane bulk modulus of the whole microcracked solid.

**keyword:** Fast multipole, Dual boundary element method, Effective elastic modulus, Microcracks.

## 1 Introduction

Generally speaking, there are large numbers of microcracks existing in brittle or quasi-brittle materials. The microcracks play an important role in the stiffness, reliability and failure behaviors of the materials. Some micromechanics methods (e.g., the dilute solution (Kachanov, 1992), the self-consistent method (Budiansky and O'Connell, 1976), the differential method (Norris, 1985), the Mori-Tanaka method (Benveniste, 1987), the generalized self-consistent method (Huang, Hu and Chanadra, 1994) and the method proposed by Feng and Yu (2000)) have been established to estimate the effective properties of microcracked solids. All these micromechanics methods depend on the statistical average effects of many microcracks and adopt the crack density as the single parameter to characterize the microcracked solids.

To investigate directly the interaction among multiple microcracks in consideration of their sizes, locations and orientations, some numerical schemes have been developed. Kachanov (1987) developed a pseudotraction method for 2D analysis. In this method the unknown crack line tractions are approximated by their average. Toi and Atluri (1990a, 1990b, 1990c) proposed a finite element analysis of the static and dynamic fracture behavior in brittle microcracking solids. In their work, stationary and propagating cracks under static and dynamic loading were simulated using a continuum constitutive modeling, and the microcrack toughening effect was discussed. Huang, et al. (1996) gave a numerical hybrid BEM method in conjunction with a unit cell model to compute the effective moduli of 2D microcracked solids. The results shows that the differential method provide the most accurate estimation at low crack density and the generalized self-consistent method is much more accurate at relatively high crack density. Zhan, Wang and Han (1999) presented a method based on a superposition scheme and series expansions of the complex potentials to directly account for the interactions of microcracks and the effect of the outer boundary in a finite plate.

Because of the boundary-only discretization and semi-analytical nature, the boundary element method (BEM) is recognized as a powerful tool for fracture mechanics analysis (Cruse, 1996). But the BEM formulation for crack problems concerns the geometry including two coincide surfaces, which cause the displacement boundary integral equation to degenerate into a singular form. The dual boundary element method (DBEM) (Portela and Aliabadi, 1992; Portela, Aliabadi and Rooke, 1993) overcomes this mathematical degeneration by using the displacement boundary integral equation for collocation on one crack surface and the traction boundary integral equation on the other. Based on the DBEM, a single-region formulation can be developed to solve general crack problems.

The conventional BEM is not efficient for large-scale problems because of its dense and asymmetric coefficient

<sup>1</sup> Dept. Engineering Mechanics, Tsinghua Univ., Beijing, China

<sup>2</sup> Correspondence author

matrix. To achieve more run-time and memory storage efficiency, the fast multipole method (FMM) (Barnes and Hut, 1986; Greengard and Rokhlin, 1997) is applied to BEM. The fast multipole BEM uses the same discretization as the conventional BEM, while uses a quad-tree (for 2D problems) or an octal-tree (for 3D problems) for computation and storage. The matrix-vector product is obtained by recursive operations on the tree structure without explicitly forming the coefficient matrix. In recent years, the fast multipole BEM and its applications were investigated by many authors, including Peirce and Napier (1995), Popov and Power (2001), Yoshida, Nishimura and Kobayashi (2001), Aoki, Amaya, Urago et al (2004), Liu, Nishimura and Otani (2005), Wang, Yao and Wang (2005), and Wang and Yao (2005). A recent literature review on the fast multipole BEM has been given by Nishimura (2002).

A fast multipole DBEM is developed in this work for the analysis of 2D microcracked solids. The use of multipole and local expansions reduce both the computational complexity and the memory requirement to  $O(N)$ , where  $N$  is the number of DOFs. This numerical scheme is used to compute the effective in-plane bulk modulus of 2D solid models with thousands of randomly distributed microcracks. The numerical results are compared with the corresponding solutions of various micromechanics methods. And the effect of microcrack non-uniform distributions on the effective elastic moduli of the whole solid is evaluated by the fast multipole DBEM.

## 2 Dual boundary integral equations for crack analysis

Figure 1 shows a crack  $\Gamma_c$  including two coincide surfaces  $\Gamma_c^-$  and  $\Gamma_c^+$  in a 2D elastic solid  $\Omega$  surrounded by an external boundary  $\Gamma_0$ .

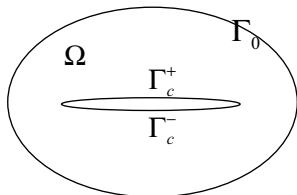


**Figure 1** : A 2D elastic solid with a single crack

In the absence of body forces, the following displacement

integral equation is obtained.

$$c_{\alpha\beta}(\mathbf{x})u_{\beta}(\mathbf{x}) = \int_{\Gamma_0 \cup \Gamma_c^+ \cup \Gamma_c^-} U_{\alpha\beta}(\mathbf{x}, \mathbf{y}) t_{\beta}(\mathbf{y}) d\Gamma(\mathbf{y}) - \int_{\Gamma_0 \cup \Gamma_c^+ \cup \Gamma_c^-} T_{\alpha\beta}(\mathbf{x}, \mathbf{y}) u_{\beta}(\mathbf{y}) d\Gamma(\mathbf{y}) \quad (1)$$

where  $\alpha$  and  $\beta$  denote the Cartesian components;  $u_{\beta}(\mathbf{y})$  and  $t_{\beta}(\mathbf{y})$  are respectively the displacement and traction components at field point  $\mathbf{y}$ ;  $c_{\alpha\beta}(\mathbf{x})$  is a free term depending on the shape of the boundary at the source point  $\mathbf{x}$ ;  $U_{\alpha\beta}(\mathbf{x}, \mathbf{y})$  and  $T_{\alpha\beta}(\mathbf{x}, \mathbf{y})$  respectively represent the Kelvin displacement and traction fundamental solutions, which are given as

$$U_{\alpha\beta}(\mathbf{x}, \mathbf{y}) = \frac{1}{8\pi G(1-\nu)} \left[ (3-4\nu) \ln\left(\frac{1}{r}\right) \delta_{\alpha\beta} + \frac{r_{\alpha} r_{\beta}}{r^2} \right] \quad (2)$$

$$T_{\alpha\beta}(\mathbf{x}, \mathbf{y}) = \frac{-1}{4\pi(1-\nu)r} \left\{ \frac{\partial r}{\partial n} \left[ (1-2\nu) \delta_{\alpha\beta} + \frac{2r_{\alpha} r_{\beta}}{r^2} \right] + (1-2\nu) \frac{n_{\alpha} r_{\beta} - n_{\beta} r_{\alpha}}{r} \right\} \quad (3)$$

for the plane strain case, where  $r$  is the distance from  $\mathbf{x}$  to  $\mathbf{y}$ ;  $G$  stands for the shear modulus and  $\nu$  for the Poisson's ratio.

Assuming continuity of both strains and tractions at  $\mathbf{x}$  on a smooth boundary, the following traction boundary integral equation can be obtained by differentiating Eq. (1) and applying the material constitutive relationships.

$$\frac{1}{2} t_{\beta}(\mathbf{x}) = n_{\alpha}(\mathbf{x}) \int_{\Gamma_0 \cup \Gamma_c^+ \cup \Gamma_c^-} D_{\gamma\alpha\beta}(\mathbf{x}, \mathbf{y}) t_{\gamma}(\mathbf{y}) d\Gamma(\mathbf{y}) - n_{\alpha}(\mathbf{x}) \int_{\Gamma_0 \cup \Gamma_c^+ \cup \Gamma_c^-} S_{\gamma\alpha\beta}(\mathbf{x}, \mathbf{y}) u_{\gamma}(\mathbf{y}) d\Gamma(\mathbf{y}) \quad (4)$$

where  $n_{\alpha}(\mathbf{x})$  denote the component of the outward unit normal at  $\mathbf{x}$ . Kernel functions  $D_{\gamma\alpha\beta}(\mathbf{x}, \mathbf{y})$  and  $S_{\gamma\alpha\beta}(\mathbf{x}, \mathbf{y})$ , which contain derivatives of  $U_{\alpha\beta}(\mathbf{x}, \mathbf{y})$  and  $T_{\alpha\beta}(\mathbf{x}, \mathbf{y})$  together with elastic constants, are defined by

$$D_{\gamma\alpha\beta}(\mathbf{x}, \mathbf{y}) = \frac{1}{4\pi(1-\nu)r} \times \left[ (1-2\nu) \left( \frac{r_{\alpha}}{r} \delta_{\beta\gamma} + \frac{r_{\beta}}{r} \delta_{\alpha\gamma} - \frac{r_{\gamma}}{r} \delta_{\alpha\beta} \right) + 2 \frac{r_{\alpha} r_{\beta} r_{\gamma}}{r^3} \right]$$

$$\begin{aligned}
S_{\gamma\alpha\beta}(\mathbf{x}, \mathbf{y}) = & \frac{G}{2\pi(1-\nu)r^2} \left\{ 2 \frac{\partial r}{\partial n} \left[ (1-2\nu) \frac{r_\gamma}{r} \delta_{\alpha\beta} \right. \right. \\
& + \nu \left( \frac{r_\alpha}{r} \delta_{\beta\gamma} + \frac{r_\beta}{r} \delta_{\alpha\gamma} \right) - 4 \frac{r_\alpha r_\beta r_\gamma}{r^3} \left. \right] \\
& + 2\nu \left( n_\alpha \frac{r_\beta r_\gamma}{r^2} + n_\beta \frac{r_\alpha r_\gamma}{r^2} \right) - (1-4\nu) n_\gamma \delta_{\alpha\beta} \\
& \left. + (1-2\nu) \left( 2n_\gamma \frac{r_\alpha r_\beta}{r^2} + n_\beta \delta_{\alpha\gamma} + n_\alpha \delta_{\beta\gamma} \right) \right\} \quad (5)
\end{aligned}$$

As the distance  $r$  tends to zero,  $S_{\gamma\alpha\beta}(\mathbf{x}, \mathbf{y})$  exhibits a hyper-singularity of the order  $1/r^2$ , while  $D_{\gamma\alpha\beta}(\mathbf{x}, \mathbf{y})$  exhibits a strong singularity of the order  $1/r$ .

Considering the following properties of the kernel functions

$$\begin{aligned}
S_{\gamma\alpha\beta}|_{\Gamma_c^+} &= -S_{\gamma\alpha\beta}|_{\Gamma_c^-}, \quad T_{\alpha\beta}|_{\Gamma_c^+} = -T_{\alpha\beta}|_{\Gamma_c^-}, \\
D_{\gamma\alpha\beta}|_{\Gamma_c^+} &= D_{\gamma\alpha\beta}|_{\Gamma_c^-}, \quad U_{\alpha\beta}|_{\Gamma_c^+} = U_{\alpha\beta}|_{\Gamma_c^-} \quad (6)
\end{aligned}$$

and the fact that the tractions of the two coincide surfaces satisfy  $\mathbf{t}|_{\Gamma^+} = -\mathbf{t}|_{\Gamma^-}$  (for surfaces in contact) or  $\mathbf{t}|_{\Gamma^+} = \mathbf{t}|_{\Gamma^-} = 0$  (for surfaces in non-contact), Eqs (1) and (4) can be rewritten in a more simplified form in terms of the crack relative displacement as

$$\begin{aligned}
c_{\alpha\beta} u_\beta(\mathbf{x}) &= - \int_{\Gamma_c^+} T_{\alpha\beta}(\mathbf{x}, \mathbf{y}) \Delta u_\beta(\mathbf{y}) d\Gamma(\mathbf{y}) \\
&+ \int_{\Gamma_o} U_{\alpha\beta}(\mathbf{x}, \mathbf{y}) t_\beta(\mathbf{y}) - T_{\alpha\beta}(\mathbf{x}, \mathbf{y}) u_\beta(\mathbf{y}) d\Gamma(\mathbf{y}), \\
(\mathbf{x} \in \Gamma_o) \quad (7)
\end{aligned}$$

$$\begin{aligned}
\frac{1}{2} (u_a^+(\mathbf{x}) + u_a^-(\mathbf{x})) &= - \int_{\Gamma_c^+} T_{\alpha\beta}(\mathbf{x}, \mathbf{y}) \Delta u_\beta(\mathbf{y}) d\Gamma(\mathbf{y}) \\
&+ \int_{\Gamma_o} U_{\alpha\beta}(\mathbf{x}, \mathbf{y}) t_\beta(\mathbf{y}) - T_{\alpha\beta}(\mathbf{x}, \mathbf{y}) u_\beta(\mathbf{y}) d\Gamma(\mathbf{y}), \\
(\mathbf{x} \in \Gamma_c^-) \quad (8)
\end{aligned}$$

$$\begin{aligned}
\frac{1}{2} (t_\beta^+(\mathbf{x}) - t_\beta^-(\mathbf{x})) \\
= n_\alpha^+(\mathbf{x}) \int_{\Gamma_o} D_{\gamma\alpha\beta}(\mathbf{x}, \mathbf{y}) t_\gamma(\mathbf{y}) - S_{\gamma\alpha\beta}(\mathbf{x}, \mathbf{y}) u_\gamma(\mathbf{y}) d\Gamma(\mathbf{y}) \\
- n_\alpha^+(\mathbf{x}) \int_{\Gamma_c^+} S_{\gamma\alpha\beta}(\mathbf{x}, \mathbf{y}) \Delta u_\gamma(\mathbf{y}) d\Gamma(\mathbf{y}), \quad (\mathbf{x} \in \Gamma_c^+) \quad (9)
\end{aligned}$$

where  $\Delta u_\beta = u_\beta^+ - u_\beta^-$  are the components of the relative displacement between  $\Gamma_c^-$  and  $\Gamma_c^+$ .

Eqs (6a-6c) are the dual boundary integral equations on which the DBEM is based. The displacement equations

Eq. (7) and Eq. (8) are applied for collocation on the external boundary and one of the crack surfaces, respectively. And the traction equation Eq. (9) is applied for collocation on the other crack surface.

The concept of finite-part integral is adopted to deal with the hyper-singular integrals caused by  $S_{\gamma\alpha\beta}(\mathbf{x}, \mathbf{y})$  (Guigiani, 1992). The crack surfaces are discretized using discontinuous elements to satisfy the continuity requirements associated with finite-part integral.

Because common elements model the square root displacement variation near the crack tip inadequately, this work employs a special crack tip element incorporating the displacement variation by modification of the shape functions. It is a 3-node discontinuous element, in which the natural coordinates are  $\varepsilon_1 = -2/3$ ,  $\varepsilon_2 = 0$  and  $\varepsilon_3 = 2/3$  for the nodes and  $\varepsilon_T = 1$  for the crack tip. The shape functions take the following form

$$\begin{aligned}
N1(\varepsilon) &= \sqrt{\frac{3}{5}} \sqrt{1-\varepsilon} \varepsilon \left( \frac{9}{8} \varepsilon - \frac{3}{4} \right) \\
N2(\varepsilon) &= \sqrt{1-\varepsilon} \left( 1 - \frac{3}{2} \varepsilon \right) \left( 1 + \frac{3}{2} \varepsilon \right) \\
N3(\varepsilon) &= \sqrt{3} \sqrt{1-\varepsilon} \varepsilon \left( \frac{9}{8} \varepsilon + \frac{3}{4} \right) \quad (10)
\end{aligned}$$

The local mixed-mode SIFs are obtained from the near-crack-tip relative displacement using the one-point formula as

$$K_I^Q = \Delta u_n^P H / 2\sqrt{r}, \quad K_{II}^Q = \Delta u_s^P H / 2\sqrt{r} \quad (11)$$

where  $\mathbf{P}$  is the first node away from the crack tip  $\mathbf{Q}$ ;  $r$  is the distance from  $\mathbf{Q}$  to  $\mathbf{P}$ ;  $\Delta u_n^P$  and  $\Delta u_s^P$  are respectively the opening and sliding displacements at node  $\mathbf{P}$ ;  $H$  is a constant defined as

$$H = \begin{cases} \sqrt{\pi/2} G (1+\nu), & \text{for plane - stress case} \\ \sqrt{\pi/2} G / (1+\nu), & \text{for plane - strain case} \end{cases} \quad (12)$$

where  $G$  stands for the shear modulus and  $\nu$  the Poisson's ratio.

### 3 Formulation and implementation of the fast multiple dual BEM

#### 3.1 Multipole expansion

The kernel functions are expanded into complex Taylor series around a selected point  $\mathbf{y}_0$ . For example,  $T_{\alpha\beta}(\mathbf{x}, \mathbf{y})$

is expand into the following form

$$T_{\alpha\beta}(\mathbf{x}, \mathbf{y}) = \sum_{k=0}^{\infty} Re \left( f^{(r)}(\mathbf{x} - \mathbf{y}_0, k) g^{(r)}(\mathbf{y} - \mathbf{y}_0, k) \right) + \sum_{k=0}^{\infty} Re \left( f^{(l)}(\mathbf{x} - \mathbf{y}_0, k) g^{(l)}(\mathbf{y} - \mathbf{y}_0, k) \right) \quad (13)$$

where  $Re()$  and  $Im()$  stand for the real and imaginary parts of a complex number respectively. The source point  $\mathbf{x}$  should be far enough from  $\mathbf{y}_0$  to satisfy the inequality  $|\mathbf{y} - \mathbf{y}_0| \leq |\mathbf{x} - \mathbf{y}_0|/2$ .

Thus the integral of  $T_{\alpha\beta}(\mathbf{x}, \mathbf{y})$  on a boundary segment  $\Gamma$  are expanded into complex Taylor series as

$$\int_{\Gamma} T_{\alpha\beta}(\mathbf{x}, \mathbf{y}) \Delta u_{\beta} d\Gamma(\mathbf{y}) = \sum_{k=0}^{\infty} Re \left( f^{(r)}(\mathbf{x} - \mathbf{y}_0, k) C^{(fr)}(\mathbf{y}_0, k) \right) + \sum_{k=0}^{\infty} Re \left( f^{(l)}(\mathbf{x} - \mathbf{y}_0, k) C^{(fi)}(\mathbf{y}_0, k) \right) \quad (14)$$

where

$$f^{(r)}(\mathbf{x}, k) = \frac{Re(\mathbf{x})}{\mathbf{x}^k}, f^{(l)}(\mathbf{x}, k) = \frac{Im(\mathbf{x})}{\mathbf{x}^k}, k = 1, 2, \dots \quad (15)$$

$C^{(fr)}(\mathbf{y}_0, k)$  and  $C^{(fi)}(\mathbf{y}_0, k)$ , which are not related to the source point  $\mathbf{x}$ , are called the multipole moments centered at  $\mathbf{y}_0$ . The expansion in Eq. (14) is called multipole expansion.

### 3.2 Multipole moment to multipole moment translation

If the multipole expansion center is shifted from  $\mathbf{y}_0$  to  $\mathbf{y}_1$ , the new multipole moments can be obtained from the original ones as

$$C^{(fi)}(\mathbf{y}_1, k) = \sum_{q=0}^{k-1} C_{k-1}^q C^{(fi)}(\mathbf{y}_0, k-q) (\mathbf{y}_0 - \mathbf{y}_1)^q + i \sum_{q=0}^{k-2} C_{k-2}^q \left[ Re(\mathbf{y}_1 - \mathbf{y}_0) C^{(fr)}(\mathbf{y}_0, k-q-1) \right] (\mathbf{y}_0 - \mathbf{y}_1)^q + i \sum_{q=0}^{k-2} C_{k-2}^q \left[ Im(\mathbf{y}_1 - \mathbf{y}_0) C^{(fi)}(\mathbf{y}_0, k-q-1) \right] (\mathbf{y}_0 - \mathbf{y}_1)^q \quad (16)$$

This translation is called multipole moment to multipole moment translation (M2M).

### 3.3 Local expansion

In the local expansion, the integral of  $T_{\alpha\beta}(\mathbf{x}, \mathbf{y})$  on  $\Gamma$  is expanded with respect to source point  $\mathbf{x}$  around a selected point  $\mathbf{x}_0$  as

$$\int_{\Gamma} T_{\alpha\beta}(\mathbf{x}, \mathbf{y}) \Delta u_{\beta} d\Gamma(\mathbf{y}) = \sum_{k=0}^{\infty} Re \left( l^{(r)}(\mathbf{x} - \mathbf{x}_0, k) D^{(lr)}(\mathbf{x}_0, k) \right) + \sum_{k=0}^{\infty} Re \left( l^{(l)}(\mathbf{x} - \mathbf{x}_0, k) D^{(li)}(\mathbf{x}_0, k) \right) \quad (17)$$

where,

$$l^{(r)}(\mathbf{x}, k) = Re(\mathbf{x}) \mathbf{x}^k, l^{(l)}(\mathbf{x}, k) = Im(\mathbf{x}) \mathbf{x}^k, k = 0, 1, 2, \dots \quad (18)$$

$D^{(lr)}(\mathbf{x}_0, k)$  and  $D^{(li)}(\mathbf{x}_0, k)$ , which are called the local moments centered at  $\mathbf{x}_0$ , can be obtained from the multipole moments centered at  $\mathbf{y}_0$  as

$$D^{(li)}(\mathbf{x}_0, l) = (\mathbf{y}_0 - \mathbf{x}_0)^{-l} \sum_{k=1}^p C_{l+k-1}^{k-1} (\mathbf{x}_0 - \mathbf{y}_0)^{-k} C^{(fi)}(\mathbf{y}_0, k) + i (\mathbf{y}_0 - \mathbf{x}_0)^{-l-1} \sum_{k=1}^p C_{l+k}^{k-1} (\mathbf{x}_0 - \mathbf{y}_0)^{-k} \times Re(\mathbf{x}_0 - \mathbf{y}_0) C^{(fr)}(\mathbf{y}_0, k) + i (\mathbf{y}_0 - \mathbf{x}_0)^{-l-1} \sum_{k=1}^p C_{l+k}^{k-1} (\mathbf{x}_0 - \mathbf{y}_0)^{-k} \times Im(\mathbf{x}_0 - \mathbf{y}_0) C^{(fi)}(\mathbf{y}_0, k) \quad (19)$$

where  $p$  is the order of the truncated series. This translation is called multipole moment to local moment translation (M2L).

### 3.4 Local to local translation

If the center of local expansion is shifted from  $\mathbf{x}_0$  to  $\mathbf{x}_1$ , the new local-expansion coefficients can be obtained from the original ones as

$$D^{(li)}(\mathbf{x}_1, l) = \sum_{k=l}^p C_k^l (\mathbf{x}_1 - \mathbf{x}_0)^{k-l} D^{(li)}(\mathbf{x}_0, k) + i \sum_{k=l+1}^p C_k^{l+1} (\mathbf{x}_1 - \mathbf{x}_0)^{k-l-1} Re(\mathbf{x}_1 - \mathbf{x}_0) D^{(lr)}(\mathbf{x}_0, k) + i \sum_{k=l+1}^p C_k^{l+1} (\mathbf{x}_1 - \mathbf{x}_0)^{k-l-1} Im(\mathbf{x}_1 - \mathbf{x}_0) D^{(li)}(\mathbf{x}_0, k) \quad (20)$$

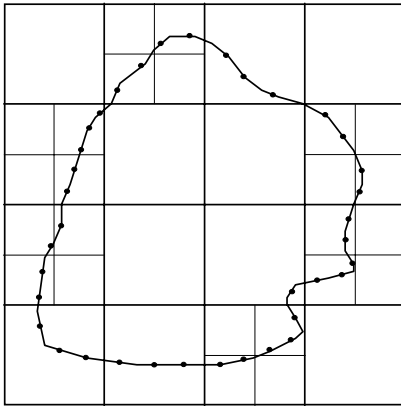


**Figure 2 :** A quad-tree structure

This translation is called local to local translation (L2L).

### 3.5 Numerical implementation of the fast multipole dual BEM

In the fast multipole DBEM, firstly the boundaries of the model are discretized using boundary elements. Only one surface of an arbitrary crack needs to be discretized. Secondly an adaptive quad-tree structure is constructed. The root of the tree, which is at level 0, is a square cell containing all the boundaries of the model. The root cell is divided into four child cells at level 1. Each child cell is divided in the same way until the number of elements in it is less than a predefined number. A childless cell is called a *leaf*. An example is shown in Figure 2, where each leaf contains at most three elements. Two cells at the same level are called *colleagues* or *well separated* if they share a boundary point or not. Among the cells well separated from cell A, those whose parents are colleagues of A's parent compose the *interaction list* of A (see Figure 3).

Then an iterative process is executed to solve the boundary integral equations. In each iterative step, the multipole and local moments are computed by some recursive operations. This work adopted the generalized minimum residual method (GMRES) as iterative solver and the sparse approximate inverse type as the preconditioner (Vavasis, 1992).

For a leaf, the multipole moments are obtained from all the elements in it using multipole expansions. For a non-leaf cell, the multipole moments are obtained from its children using M2M. The M2M translation is executed upward to level 2.

The local moments of a cell A are a sum of two parts.

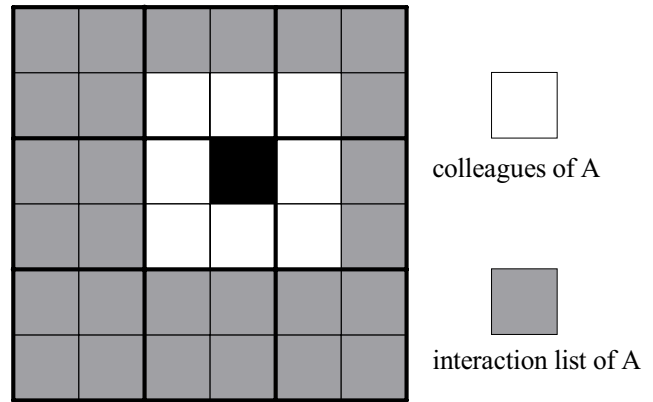


**Figure 3 :** The colleagues and interaction list of cell A

One part is obtained from the multipole moments of A's interaction list using M2L and the other from the local moments of A's parent using L2L. This operation is executed downward until leaves are reached.

For a source point  $\mathbf{x}$  in leaf A, the boundary integral is calculated in two parts. The contribution of the elements in A and A's colleagues is evaluated in the same way as the conventional BEM, while the contribution of all other elements is obtained from the local expansion of A.

## 4 Numerical examples

### 4.1 Comparison of solution time between the conventional DBEM and the fast multipole DBEM

Various numbers of periodically located microcracks in a rectangular plate were analyzed using the conventional DBEM and the fast multipole DBEM respectively. In the fast multipole DBEM analysis, the order of the finite series was taken as  $p = 20$ . Figure 4 compares the total CPU time for various problem sizes by the fast multipole DBEM with the corresponding data by the conventional DBEM, which employs an ordinary Gauss elimination solver using the famous Lapack library. The results show that the fast multipole DBEM is much more efficient than the conventional DBEM for large-scale problems.

### 4.2 Simulation of a plate with $n \times n$ periodically located microcracks

This example simulated a plate composed of  $n \times n$  square cells as shown in Figure 5. There is a horizontally oriented microcrack in the center of each square cell. The value of  $n$  was varied from 5 to 100. The width of each

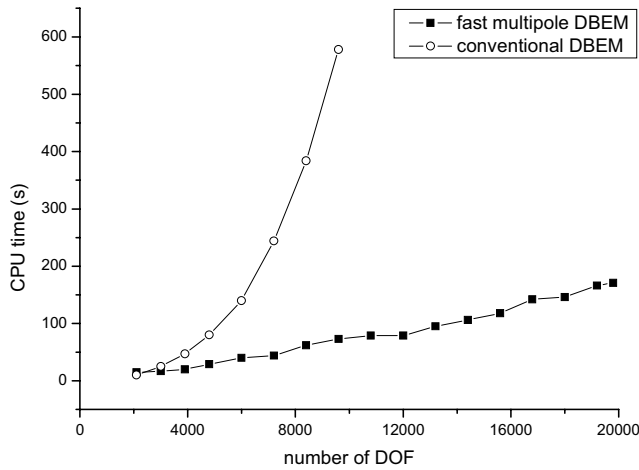


**Figure 4 :** Comparison of solution speed between conventional BEM and fast multipole BEM

square cell is  $2w = 5\text{mm}$ , the crack length is  $2a = 2\text{mm}$ , and the Young’s modulus and Poisson’s ratio of the matrix material are  $E = 200\text{GPa}$ ,  $\nu = 0.3$ , respectively. The four sides of the plate are given uniform normal-direction displacement  $\bar{u}_n = n \times 0.1\text{mm}$ . So theoretically all the crack tips must have the same SIFs when  $n$  is set as different values.

This example is considered as a plane-stress problem. In numerical analysis, each crack was divided into 16 discontinuous quadratic elements and the order of finite series was taken as  $p = 25$ . Table 1 shows the SIF results for different values of  $n$ .  $K_{I\text{max}}$  and  $K_{I\text{min}}$  are respectively the maximum and minimum among the  $K_I$  values of all the crack tips. The numerical results prove that the fast multipole DBEM scheme can achieve high accuracy even for large-scale problems.

**Table 1 :** SIF results of  $n \times n$  periodically oriented microcracks in a square plate

Number of cracks	Number of DOFs	$K_{I\text{max}}$ (Mpa mm <sup>1/2</sup> )	$K_{I\text{min}}$ (Mpa mm <sup>1/2</sup> )
5×5	7,200	16576	16576
10×10	19,200	16576	16577
20×20	57,600	16576	16577
50×50	288,000	16575	16577
100×100	1,056,000	16578	16582

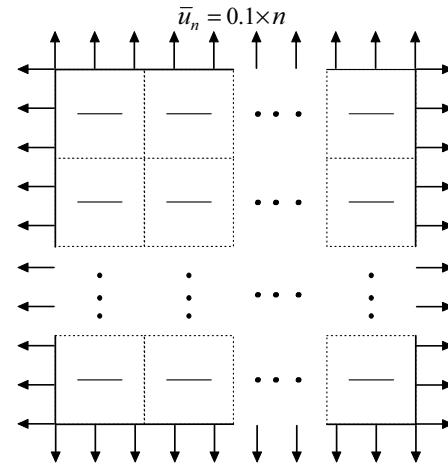


**Figure 5 :** A square plate with  $n \times n$  periodically located microcracks

## 5 Computation of effective elastic moduli

### 5.1 The numerical model for computation of effective in-plane bulk modulus

Figure 6 shows the model for computation of effective in-plane bulk modulus.  $\Gamma_1$  and  $\Gamma_2$ , which are two side of the square plate, are given uniform normal displacement  $\bar{u}_n$ . For 2D cases, the average stresses are obtained from the tractions on  $\Gamma_1$  and  $\Gamma_2$ , as

$$\bar{\sigma}_{11} = \frac{1}{L} \int_{\Gamma_1} T_1 d\Gamma, \quad \bar{\sigma}_{22} = \frac{1}{L} \int_{\Gamma_2} T_2 d\Gamma \quad (21)$$

where  $L$  is the length of the plate.

The average strains of the plate are calculated as

$$\bar{\epsilon}_{11} = \bar{u}_n/L, \quad \bar{\epsilon}_{22} = \bar{u}_n/L \quad (22)$$

Then the in-plain bulk modulus of the microcrack plate is obtained as

$$K_e = (\bar{\sigma}_{11} + \bar{\sigma}_{22})/2(\bar{\epsilon}_{11} + \bar{\epsilon}_{22}) \quad (23)$$

The in-plane bulk modulus of the matrix material can be determined as

$$K_0 = \begin{cases} E_0/2(1 + \nu_0)(1 - 2\nu_0) & \text{(for plane - strain case)} \\ E_0/2(1 - \nu_0) & \text{(for plane - stress case)} \end{cases} \quad (24)$$

where  $E_0$  and  $\nu_0$  are respectively the Young’s modulus and the Poisson ratio of the matrix material.

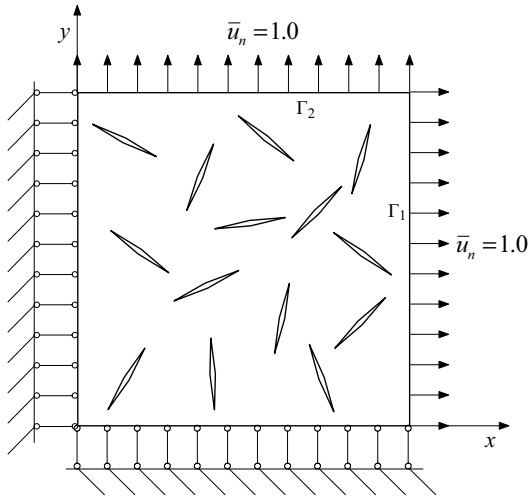


**Figure 6 :** The model for computation of effective in-plane bulk modulus

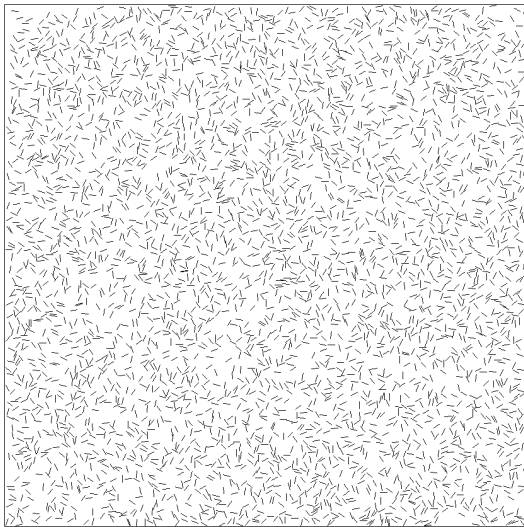


**Figure 8 :** A square plate containing 4,000 randomly oriented microcracks

Following Budiansky and O’Connell (1976), the crack density for a 2D microcracked solid is defined as

$$\omega = \frac{1}{A} \sum_{i=1}^N a_i^2, \quad (25)$$

where  $A$  is the area of the 2D solid,  $N$  is the number of the microcracks, and  $a_i$  is the half-length of the  $i$ -th microcrack.

In the computation of effective elastic moduli, an important criterion is the convergence of the calculation as the number of microcracks increases. Figure 7 shows the results of the convergence test for a crack density  $\omega = 0.2$ ,

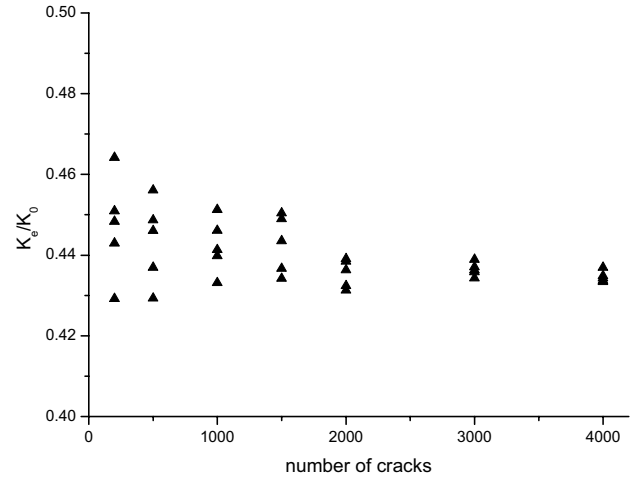


**Figure 7 :** The convergence test for a crack density  $\omega = 0.2$

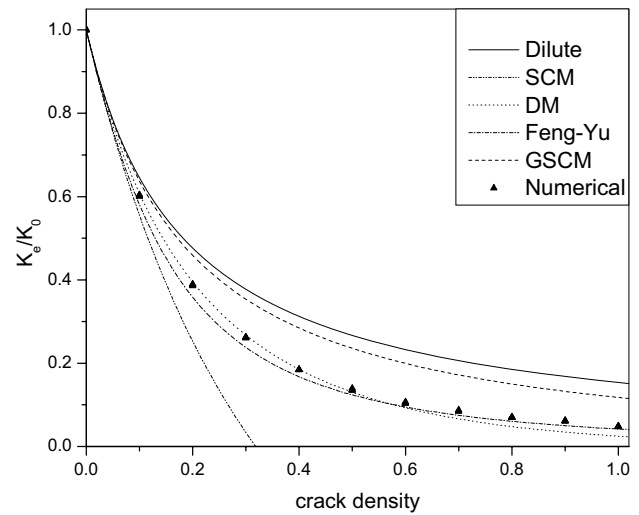


**Figure 9 :** Effective in-plane bulk modulus versus crack density

with the Poisson’s ratio  $\nu = 0.3$ .

Five different specimens were analyzed for each fixed number of microcracks. The numerical analysis was limited to plane-strain case. The results show that the effective in-plane bulk modulus tends to be stable when the number is greater than 2000.

### 5.2 The effective in-plane bulk modulus of a microcracked solid

The fast multipole DBEM is adopted to directly determine the effective in-plane bulk modulus of a square plate containing 4,000 randomly oriented microcracks, as shown

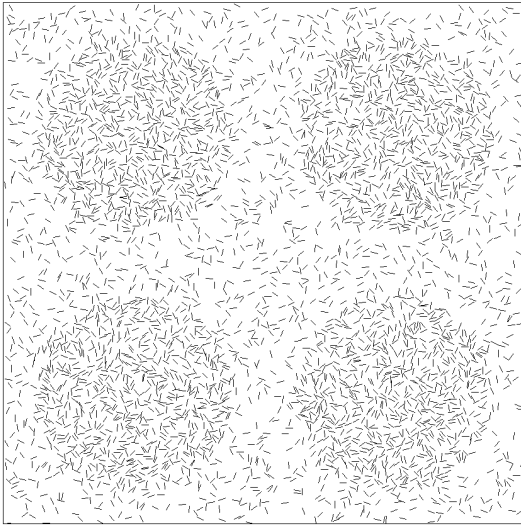


**Figure 10** : A square plate containing four local regions

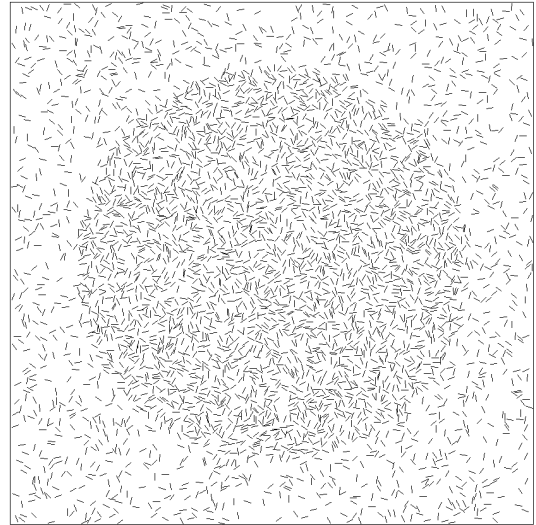


**Figure 11** : A square plate containing one local region

in Figure 8. The crack density is varied from 0.1 to 1.0 by changing the crack size. For each fixed crack density, five different specimens were analyzed. The numerical analysis was limited to plane-strain case. Because of the large number of the microcracks, there is no obvious difference among the results of specimens with the same crack density.

Figure 9 shows the numerical results of the effective in-plane bulk modulus by the fast multipole DBEM in comparison with the corresponding solutions of various micromechanics methods, with the Poisson's ratio  $\nu = 0.3$ . Only the following micromechanics methods are considered, i.e. the dilute solution, the self-consistent method (SCM), the differential method (DM), the generalized self-consistent method (GSCM), and the method proposed by Feng and Yu (2000).

From the comparison of numerical results and estimates of micromechanics methods, the following valuable conclusions can be obtained:

- (1) The numerical results by the fast multipole DBEM scheme agree well with the estimations of GSCM, DM, and Feng-Yu. Especially, Feng-Yu method is the most accurate among all the five micromechanics methods since the difference between the numerical results and Feng-Yu estimation is very small even at high crack density.
- (2) Compared with the numerical scheme and other micromechanics methods, the dilute solution and the self-consistent method lead to larger error. They give acceptable estimations only at relative low crack density.

### 5.3 Effect of crack non-uniform distribution on effective in-plane bulk modulus

Estimates of effective elastic moduli using the above micromechanics methods are based on the assumption that the microcracks are uniformly distributed in the matrix material. In this section, the effect of crack non-uniform distributions is discussed. This work assumes that the microcracked solid contains some local regions having a crack density  $\omega_L$  higher or lower than the average crack density  $\omega_0$  and analyze the variation of the effective in-plane modulus with  $\omega_L$  when  $\omega_0$  is fixed.

This work uses two non-uniform distribution models. The first model is a square plate containing four identical circular local regions, as shown in Figure 10. The diameter of the circles  $d = 0.375L$ , where  $L$  is the width of the square plate. The second model, as shown in Figure 11, contains one circular local region with the diameter  $d = 0.75L$ .

The results for the average crack density  $\omega_0 = 0.2$  and  $\omega_0 = 0.3$  are shown in Figures 12-15 respectively, with the Poisson's ratio  $\nu = 0.3$ . For each value of  $\omega_L$ , five different specimens were created and analyzed. The numerical analysis was limited to plane-strain case.

From Figures 12-15, it can be found that the effective in-plane bulk modulus  $K_e$  reach minimum when  $\omega_L$  is near to  $\omega_0$ , while  $K_e$  exhibits obvious rise when  $\omega_L$  is higher or lower than  $\omega_0$ . The results show that the non-uniform distributions of microcracks increase the effective in-plane bulk modulus of the whole microcracked

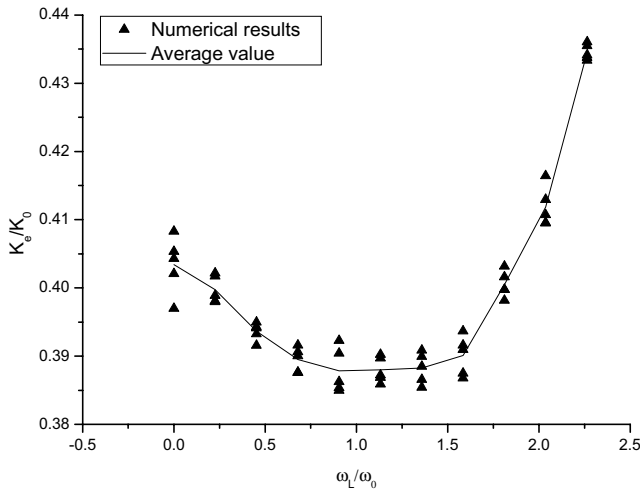


**Figure 12 :**  $K_e/K_0$  versus  $\omega_L/\omega_0$  for the model containing one local region ( $\omega_0 = 0.2$ )

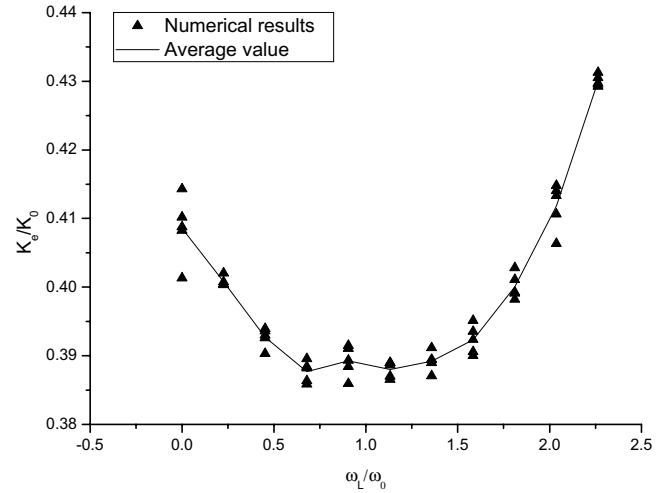


**Figure 13 :**  $K_e/K_0$  versus  $\omega_L/\omega_0$  for the model containing four local regions ( $\omega_0 = 0.2$ )

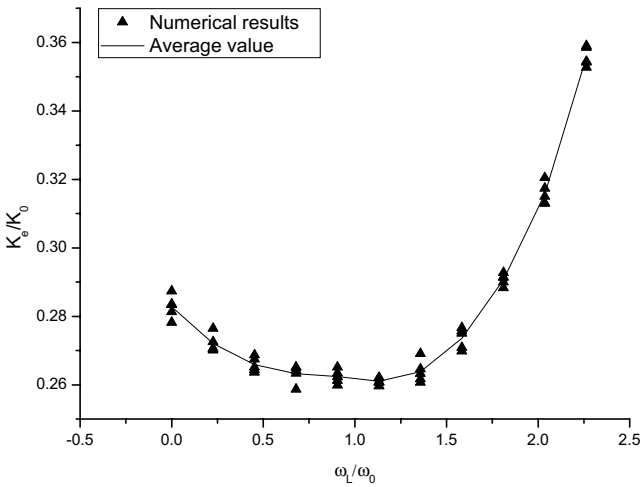


**Figure 14 :**  $K_e/K_0$  versus  $\omega_L/\omega_0$  for the model containing one local region ( $\omega_0 = 0.3$ )

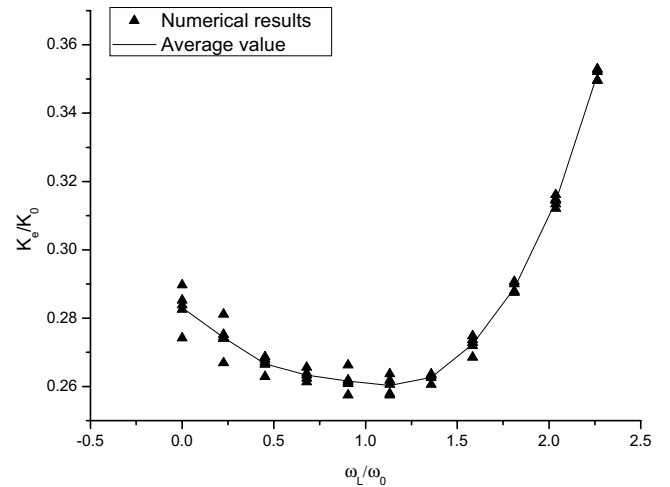


**Figure 15 :**  $K_e/K_0$  versus  $\omega_L/\omega_0$  for the model containing four local regions ( $\omega_0 = 0.3$ )

solid.

## 6 Conclusions

FMM based on complex Taylor series expansions was applied to DBEM for the analysis of finite solids with large numbers of microcracks. Combining multipole expansions with local expansions, the run-time and memory efficiency were significantly enhanced. Some numerical examples show that the presented numerical scheme can achieve high accuracy and high efficiency in the analysis of microcracked solids.

The fast multipole DBEM was used to determine the effective in-plane bulk modulus of 2D solid models con-

taining thousands of randomly distributed microcracks. The numerical results were compared with the corresponding solutions of various micromechanics methods. The comparison proves that the generalized self-consistent method, the differential scheme, and Feng and Yu's method can provide satisfactory estimations and especially Feng and Yu's method can give very accurate solutions even if the crack density is relative high.

In addition, the presented fast multipole DBEM was used to evaluate the effect of microcrack non-uniform distribution on the effective elastic modulus. This work analyzed 2D microcracked solids containing some local regions having a crack density higher or lower than the average

crack density. And the numerical results show that the non-uniform distribution of microcracks increases the effective in-plane bulk modulus of the whole microcracked solid.

**Acknowledgement:** Financial support for the projects from the National Natural Science Foundation of China, under grant No. 10172053, 10472051 and the project from the Ministry of Education is gratefully acknowledged.

## References

- Aoki, S.; Amaya, K.; Urago, M. et al.** (2004): Fast multipole boundary element analysis of corrosion problems. *CMES-Comput. Model. Eng. Sci.*, vol. 6, No. 2, pp. 123-131.
- Barnes, J.; Hut, P. A.** (1986): Hierarchical  $O(N \log N)$  force calculation algorithm. *Nature*, vol. 324, pp. 446-449.
- Benveniste, Y.** (1987): A new approach to the application of Mori-Tanaka's theory in composite materials. *Mech. Mater.*, vol. 6, pp. 147-157.
- Budiansky, B.; O'Connell, R. J.** (1976): Elastic moduli of a cracked solid. *Int. J. Solids. Struct.*, vol. 12, pp. 81-95.
- Cruse, T. A.** (1996): BIE fracture mechanics analysis 25 years of developments. *Comput. Mech.*, vol. 18, No. 1, pp. 1-11.
- Feng, X. Q.; Yu, S. W.** (2000): Estimate of effective elastic moduli with microcrack interaction effects. *Theor. Appl. Fract. Mech.*, vol. 34, pp. 225-233.
- Greengard, L.; Rokhlin, V.** (1997): A fast algorithm for particle simulation. *J. Comput. Phys.*, vol. 35, pp. 280-292.
- Guiggiani, M.** (1992): A general algorithm for the numerical solution of hypersingular boundary integral equations. *J. Appl. Mech.*, vol. 59, pp. 604-614.
- Huang, Y.; Chandra, A.; Jiang, Z. Q.; Wei, X.; Hu, K. X.** (1996): The numerical calculation of two-dimensional effective moduli for microcracked solids. *Int. J. Solids. Struct.*, vol. 33, pp. 1575-1586.
- Huang, Y.; Hu, K. X.; Chanadra, A.** (1994): A generalized self-consistent mechanics method for microcracked solids. *J. Mech. Phys. Solids*, vol. 42, pp. 1273-1291.
- Kachanov, M.** (1987): Elastic solids with many cracks: a simple method of analysis. *Int. J. Solids. Struct.*, vol. 23, pp. 23-43
- Kachanov, M.** (1992): Effective elastic properties of cracked solids: critical review of some basic concepts. *Appl. Mech. Rev.*, vol. 45, pp. 304-335.
- Liu, Y. J.; Nishimura, N.; Otani, Y.** (2005): Large-scale modeling of carbon-nanotube composites by a fast multipole boundary element method. *Comput. Mater. Sci.*, vol. 34, No. 2, pp. 173-187.
- Nishimura, N.** (2002): Fast multipole accelerated boundary integral equation methods. *Appl. Mech. Rev.*, vol. 55, No. 4, pp. 299-324.
- Norris, A. N.** (1985): A differential scheme for the effective moduli of composites. *Mech. Mater.*, vol. 4, pp. 1-16.
- Peirce, A. P.; Napier, J. A. L.** (1995): A spectral multipole method for efficient solutions of large scale boundary element models in elastostatics. *Int. J. Num. Meth. Eng.*, vol. 38, pp. 4009-4034.
- Popov, V.; Power, H.** (2001): An  $O(N)$  Taylor series multipole boundary element method for three-dimensional elasticity problems. *Eng. Anal. Bound. Elem.*, vol. 25, pp.7-18.
- Portela, A.; Aliabadi, M. H.** (1992): The dual boundary element method: effective implementation for crack problems. *Int. J. Num. Meth. Eng.*, vol. 33, pp. 1269-1287.
- Portela, A.; Aliabadi, M. H.; Rooke, D. P.** (1993): Dual boundary element incremental analysis of crack propagation. *Comput. Struct.*, vol. 46, No. 2, pp. 237-247.
- Toi, Y.; Atluri, S. N.** (1990a): Finite Element Analysis of Static and Dynamic Fracture of Brittle Microcracking Solids, Part 1:-Formulation and Simple Numerical Examples. *Int. J. Plasticity*, Vol. 6, pp. 169-188.
- Toi, Y.; Atluri, S. N.** (1990b): Finite Element Analysis of Static and Dynamic Fracture of Brittle Microcracking Solids, Part 2:-Stationary and Growing Macro-Cracks Under Static Loading. *Int. J. Plasticity*, Vol. 6, pp. 263-280.
- Toi, Y.; Atluri, S. N.** (1990c): Finite Element Analysis of Static and Dynamic Fracture of Brittle Microcracking Solids, Part 3:-Stationary and Rapidly Propagating Cracks Under Dynamic Loading. *Int. J. Plasticity*, Vol. 6, pp. 389-414.

**Vavasis, S. A.** (1992): Preconditioning for boundary integral equations. *SIAM J. Matrix. Anal. Appl.*, vol. 13, No. 3, pp. 905-925.

**Wang, H. T.; Yao, Z. H.; Wang, P. B.** (2005): On the preconditioners for fast multipole boundary element methods for multi-domain elastostatics in 2D. *Eng. Anal. Bound. Elem.*, vol. 29, No. 7, pp. 673-688.

**Wang, H. T.; Yao, Z. H.** (2005): A new fast multipole boundary element method for large scale analysis of mechanical properties in 3D particle-reinforced composites. *CMES-Comput. Model. Eng. Sci.*, vol. 7, No. 1, pp. 85-96.

**Yoshida, K.; Nishimura, N.; Kobayashi, S.** (2001): Application of new fast multipole boundary integral equation method to crack problems in 3D. *Eng. Anal. Bound. Elem.*, vol. 25, pp. 239-247.

**Zhan, S.; Wang, T.; Han, X.** (1999): Analysis of two dimensional finite solids with microcracks. *Int. J. Solids. Struct.*, vol. 36, pp. 3775-3753.

